Science
AAAS

Supplementary Materials for

Trained ILC3 responses promote intestinal defense

Nicolas Serafini *et al*.

Corresponding author: James P. Di Santo, james.di-santo@pasteur.fr

Science **375**, 859 (2022)
DOI: 10.1126/science.aaz8777

The PDF file includes:

Other Supplementary Material for this manuscript includes the following:

MATERIALS and METHODS

Mice

Gender- and age-matched mice between 6 to 12 weeks of age were used. *Rorc*$^{gfp/+}$ (*16*), *Il22*$^{TdT/+}$ (*17*), *Id2*^{CreERT2} (*22*), and *Il22*$^{-/-}$ mice (*36*) have been previously described. *Rag2*$^{-/-}$*IL2rg*$^{-/-}$ mice were maintained at CDTA (Orléans, France), while all other strains were housed at the Institut Pasteur. *Rorc*^{GFP} and *Rosa26*^{RFP} mice were provided by G. Eberl (Institut Pasteur, Paris, France). All mice were on the C57BL/6 background and were maintained under specific pathogen-free conditions, provided with food and water ad libitum. To generate *Id2*^{RFP} mice, *Id2*^{CreERT2} mice were crossed with *Rosa*26^{RFP} mice. Where noted, tamoxifen (10 mg/ml in 10% ethanol in Corn oil; 100 mg/kg) was administrated by daily intraperitoneal injection during 4 consecutive days. Mice were transferred and maintained in the A3 isolators prior to infection. For antibiotic treatment, mice were treated 3 days with ciprofloxacin (Sigma Aldrich; 200 µl in H_2O; 100 mg/kg/day) 4 days after *C. rodentium* infection. Experimental animal protocols were performed in accordance with the guidelines of the Animal Care Use Committee at the Institut Pasteur and were approved by the French Research Ministry (project #2013-0033).

C. rodentium infection and imaging

The bioluminescent *Citrobacter rodentium* strain IC180 was used in this study (*37*). Log-phase cultures of bacteria were growth from overnight culture, washed in PBS and mice were orally infected with 10^9 colony-forming unit (CFU) as previously described (*16*). Animals were monitored for survival, suffering and were weighed periodically. Feces were collected from live mice and homogenized in sterile PBS, following infection and/or antibiotic treatment. The bacterial load was determined by plating serial dilutions of the homogenates on LB agar plates. For in vivo tracking of *C. rodentium*, mice were anaesthetized, and the abdominal region was shaved. Mice were placed in a confinement box with oxygen (TEM SEGA) and imaged using an IVIS 100 system (Caliper Life Sciences). Image acquisition and analysis were performed with the Living Image 3.2 software (Caliper Life Sciences) as described (*38*).

L. monocytogenes (LM) infection

LM were grown from overnight culture and then diluted in brain-heart infusion medium to reach mid-log growth phase as previously described (*28*). Bacteria were washed in PBS and mice were then orally infected with 10^9 CFU as previously described (*6*). Animals were monitored for survival, suffering and were weighed periodically.

Isolation of cells from intestinal tissue and ex vivo stimulation

Small intestines were collected from euthanized mice. Peyer's patches were removed and intestinal epithelial cells were eliminated by shaking incubation in 0.5 mM EDTA and 1 mM Hepes (Sigma Aldrich) for 20 min at 37°C. Subsequently, the intestinal tissue was minced and incubated two times in a digestion solution containing 0.5 mg/ml collagenase VII (Sigma-Aldrich) for 20 min at 37°C in a shaking incubator to isolate the lamina propria lymphocytes (LPL). LPLs were further purified using a 40% Percoll, filtered through a 70µm nylon mesh and kept in 10% FCS RPMI. For cytokine ex-vivo stimulation, 1-5×10^6 cells were incubated at 37°C with IL-1β (Peprotech), IL-23 (R&D Systems) at several

concentrations (see details in figure legends) and BD GolgiPlug (BD) in 10% FCS DMEM for 3 hours (37°C and 5% CO_2). To assess metabolic pathways, inhibitors were added during the stimulation: 2.5 mM [^{3}H]2-deoxy-d-glucose (2-DG), 10 mM bis-2-(5-phenylacetamido -1,3,4-thiadiazol-2-yl) ethyl sulfide (BPTES), 10mM etomoxir (E), 5 μM rotenone (R), 5 μM antimycin A (AA), 2 nM oligomycin A (O; all from Sigma), and 0.5 mM Nω-hydroxy-L-arginine (Nor-NOHA; N; Cayman chemical). To assess the OXPHOS inhibition impact, ILC3 were cultured with IL-7, Flt3-L, SCF (20 ng/ml), IL-23 and IL-1β (25 ng/ml) in DMSO or 5 μM AA, 5 μM R and 2 nM O for 18 hours and IL-22 production was analyzed by flow cytometry

Flow Cytometry

For flow cytometry analysis, single-cell suspensions were stained with Flexible Viability Dye eFluor 506 (eBioscience) and blocked with FcR Blocking Reagent (Miltenyi) for 15 min, followed by 30 min of surface-antigen staining with a combination of fluorescently conjugated monoclonal antibodies on ice. For experiments involving intracellular and intranuclear transcription factor staining, cells were fixed, permeabilized, and stained using BD Transcription Factor Staining kit and Foxp3/Transcription Factor Staining Buffer Kit respectively, according to the manufacturer's instructions (BD Biosciences and eBioscience). The following antibodies were used for the study: CCR6 BV421 (140706, BD Biosciences), CD11b AF700 (M1/70, eBioscience), CD11c APC (N418; eBioscience), Siglec-F PE-TxR (E50-2440; BD Biosciences), Ly6G AP-Cy7 (1A8; Biolegend), Ly6C FITC (AL-21, BD Biosciences), F4/80 PE-cy7 (BM8, eBioscience), IA/IE Pac-Blue (M5/114.15.2, BD Biosciences), CD19 PerCP-Cy5.5 (1D3, BD Biosciences), CD127 PE-Cy7 (A7R34, eBioscience), CD3 APC (145-2C11, eBioscience), CD3 eF450 (500A2, eBioscience), CD3 BUV737 (17A2, BD Biosciences), CD44 Bv786 (IM7; BD Biosciences), CD45 BUV395 (30-F11, BD Biosciences), CD45.1 APC-Cy7 (A20, BD Biosciences), CD45.2 APC-eF780 (104, eBioscience), CD45.2 BV711 (104, BD Biosciences), CD45.2 FITC (104, BD Biosciences), CD5 APC-R700 (53-7.3, BD Biosciences), CD49a BV711 (Ha31/8, BD Biosciences), CD5 BV605 (53-7.3, BD Biosciences), CD62L APC-Cy7 (MEL-14 (Biolegend), CD8α BUV805 (53-6.7, BD Biosciences), CD4 APC (GK1.5, eBioscience), CD4 A700 (RM4-5; eBioscience), CD90.2 PerCP-eF710 (30-H12, eBioscience), CD90.2 BV605 (53-2.1, Biolegend), CD90.2 FITC (53-2.1, eBioscience), KLRG1 BV605 (2F1, BD Biosciences), KLRG1 BV711 (2F1, BD Biosciences), NK1.1 APC-Cy7 (PK136, Biolegend), NK1.1 BUV395 (PK136, BD Biosciences), NKp46 APC (29A1.4, eBioscience), NKp46 PE (29A1.4, eBioscience), CD304 APC (3.E12; Biolegend) RORγt PE-CF594 (Q31-378, BD Biosciences), RORγt APC (AFKJS-9, eBioscience), IL-22 PE/APC (1H8PWSR, eBioscience), IL-22 PerCP-eF710 (IL22JOP, BD Biosciences), IFN-γ FITC (XMG1.2, BD Biosciences), IL-17A PE (TC11-18H10; BD Biosciences). Samples were acquired on a custom-configurated LSR Fortessa (BD Biosciences) and the data were analyzed on FlowJo10 software version 10 (TreeStar).

Immunofluorescence staining and confocal imaging

The small intestine was excised, washed and fixed in paraformaldehyde (Sigma-Aldrich) 4% (wt/vol) overnight followed by dehydration in 30% sucrose before embedding

in Tissue-Tek (Sakura Finetek). Samples were frozen in a bath of isopentane cooled with liquid nitrogen and were stocked at −80°C. 8µm sections were cut and adhered to Superfrost Plus slides (VWR). Frozen sections were first hydrated for 5 min in PBS containing 0.1% (vol/vol) Triton X-100 and 1% (vol/vol) normal goat serum and blocked for 1 hour at 20 °C with 10% (vol/vol) bovine serum in PBS 0.3% Triton X-100. Slides were then incubated overnight at 4°C with primary polyclonal antibody in, were washed three times, were incubated for 1 hour at 20°C with secondary conjugated antibody, then were washed once, incubated for 5 min at 20°C with DAPI (4,6-diamidino-2-phenylindole; Sigma-Aldrich), washed three times, and mounted with Fluoromount-G (Southern Biotech). The following antibodies were used for staining: anti-GFP (ab13970; Abcam), anti-RFP (600-401-379; Rockland), and anti-CD3 (clone 500A2; BD Biosciences). Slides were examined with an AxioImager Apotome microscope (Carl Zeiss).

Analysis of fecal microbiota

Feces were collected from mice, DNA extracted and sequencing of the 16S rRNA V3 region performed as previously described (*39*). We recovered from 30 samples a total of 4,466,810 reads (83.6% mapped, 102,129 mapped reads on average). The bioinformatics analysis was performed as previously described (*40*). Briefly, Operational Taxonomic Units (OTU) were clustered (threshold = 98%) with VSEARCH (v1.4), aligned to the SILVA reference database and analyzed with SHAMAN (SHiny application for Metagenomic Analysis (shaman.c3bi.pasteur.fr). Principal coordinates analysis (PCOA) based on Bray Curtis distance matrix was computed at OTU level to describe microbiota similarities.

Bulk RNA isolation and RNA-seq analysis

Cells of interest (2-12×10^4) were sorted directly in RNA lysis buffer (Qiagen) using a FACS Aria (BD Bioscience). mRNA was purified using RNeasy microkit (Qiagen) and RNA quality and integrity were analyzed using a Bioanalyser (Agilent). Samples with RNA integrity number (RIN) above 8 were used to generate cDNA. rRNA sequences were eliminated by enzymatic treatment (Zap R, Clontech). The RNAseq libraries were prepared with the Smarter Stranded Total RNA-seq Kit – Pico input mammalian (Clontech) and checked by Bioanalyzer (Agilent). Clusters were generated for the resulting libraries, with Illumina HiSeq SR Cluster Kit v4 reagents. Sequencing was performed with the Illumina HiSeq 2500 system and HiSeq SBS kit v4 reagents. Runs were carried out over 65 cycles, including seven indexing cycles, to obtain 65-bp single-end reads. Sequencing data were processed with Illumina Pipeline software (Casava version 1.9). Data were normalized and analyzed in R software with the Bioconductor packages. Pathway analysis on differentially expressed genes were identified using Reactome and Uniprot databases.

ECAR and OCR measurements

Oxygen consumption rates (OCRs) and extracellular acidification rates (ECARs) were measured for freshly sorted ILC3 (10^4 cells) from three mice for each condition using an extracellular flux analyzer (XFe96; Seahorse Bioscience) as previously described (*41*).

Adoptive ILC3 in vivo transfer

CR and CRACR mice were sacrificed on from Day 2 to 4 post-infection (or reinfection) and for each condition 1.5×10^3 intestinal ILC3 were sorted. Three days before i.v. cell transfer, *Il22*$^{-/-}$ recipient mice were infected with CR. Animals were monitored for survival, suffering and were weighed periodically.

Statistical analysis

All statistical tests were performed using Prism v.9 (GraphPad). Points in graphs indicate individual samples, bar graphs indicate means, error bars indicate individual sample SEM, and representative results are shown (as indicated in figure legends). The statistical tests employed are detailed in the figure legends. *P* values <0.05 were considered significant.

SUPPLEMENTAL FIGURES and LEGENDS

Figure S1

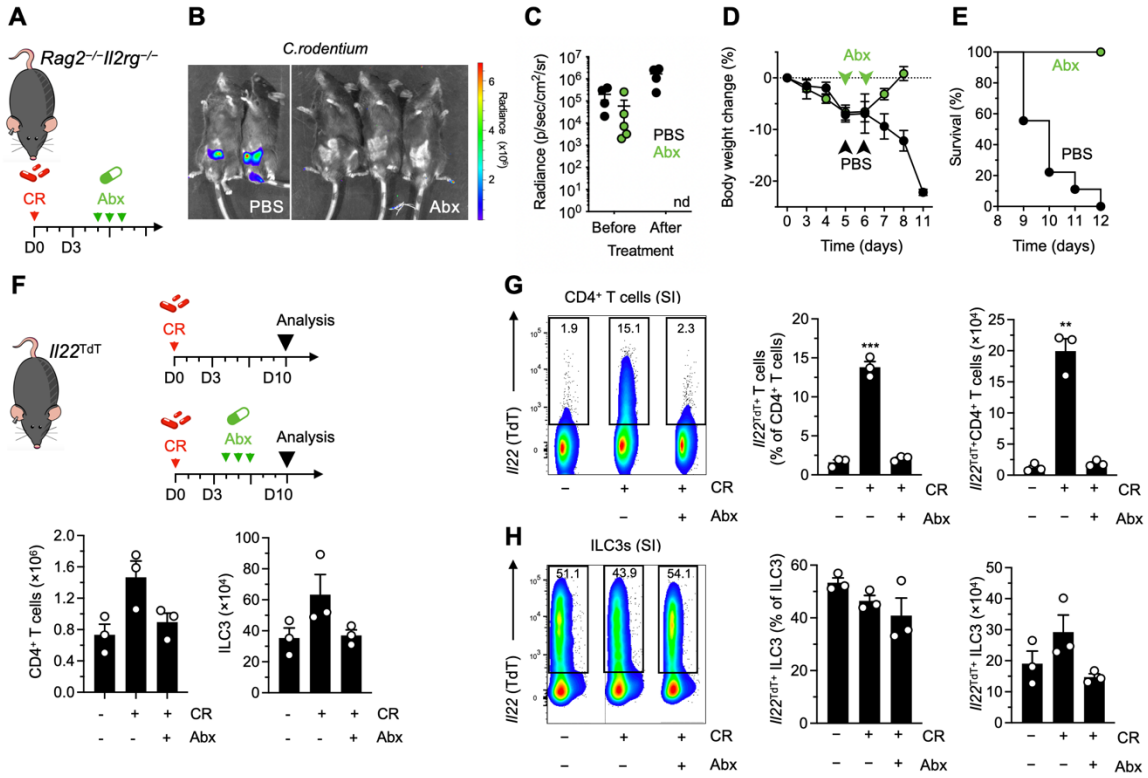

Fig. S1. ILC3 and T cell responses in CR and CRA models
(**A** to **E**). *Rag2*$^{-/-}$*Il2rg*$^{-/-}$ mice received ciprofloxacin (Abx; 100 mg/kg/day) or PBS after *C. rodentium* (CR) infection. The antibiotic was administered by oral gavage. (**B** and **C**) After infection, mice were examined for CR growth dynamics using noninvasive Xenogen technology. Representative pseudocolor images are shown (day 8; B) and average radiance analysis was calculated (C). Data are representative of two independent experiments (scale bar, photon/s/cm^2/sr; n=4-5) (**D** and **E**) Body weight (D) and survival (E) were monitored in PBS (n=8) and Abx (n=5) mice. (**F**) Infected *Il22*^{TdT} reporter mice received antibiotic treatment by oral gavage (ciprofloxacin, Abx; 100 mg/kg/day for 3 days) or PBS, 4 days after CR infection. Mice were sacrificed at day 10 after infection and absolute numbers of CD4$^+$ T cells and ILC3 were determined (n=3). (**G** and **H**) Representative flow cytometry analysis and quantification of frequencies and absolute numbers of *Il22*$^{TdT+}$ CD3$^+$CD5$^+$CD4$^+$ T cells (G; n=3) and *Il22*$^{TdT+}$ ILC3 (H; n=3). Each graph corresponds to the mean ± SEM of the values obtained (**P<0.01, *** P<0.001; two-tailed Mann-Whitney test).

Figure S2

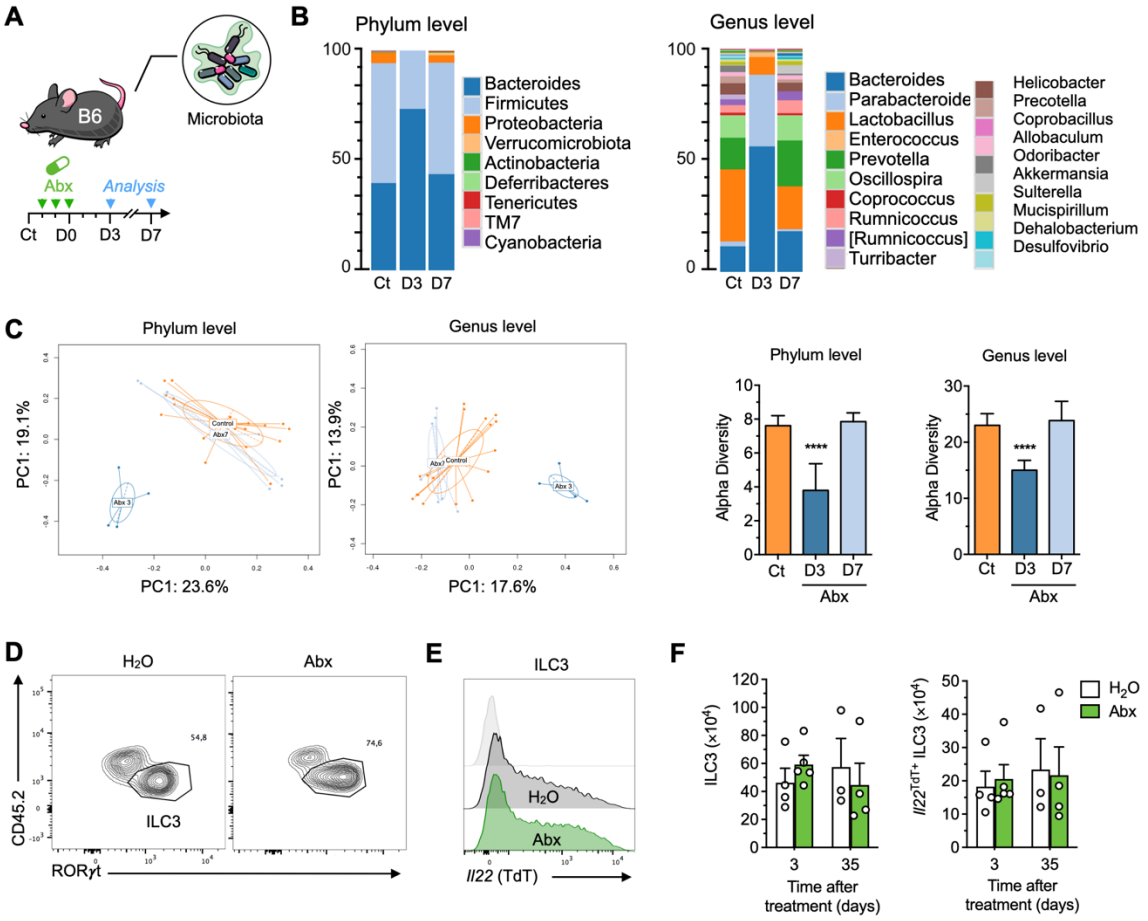

Fig. S2. Effect of antibiotic treatment on intestinal microbiota and ILC3 phenotype (**A** to **C**) C57BL/6 mice received ciprofloxacin (Abx; 100 mg/kg/day) by oral gavage. (**B**) Relative abundance of major bacterial phylum and genus in the fecal microbiota from control or Abx treated mice (3 and 7 days after administration) were quantified by 16S rRNA gene sequencing. (**C**) 16S rRNA Operational taxonomic units (OTU) are clustered according to principal-coordinate (PC) analysis of untreated and treated (3 days and 7 days after Abx treatment). Percentage of variation, using Bray Curtis distance, are indicated on the *x* and *y* axes. The alpha diversity, shown as total observed OTU and Shannon index, in untreated and treated (3 days and 7 days after Abx treatment). Mean and standard error of mean (SEM) values are indicated, and subgroups (D3, n=5; D7, n=7) are compared to control (Ct, n=18) with one-way ANOVA test followed by pairwise comparisons. **** $P<0.0001$. (**D** to **G**) Intestinal ILC3 subsets were analyzed in control and antibiotic (Abx) treated mice (D). Expression of *Il22* (TdT) in ILC3 from control (black line) and Abx treated mice (green line; E). Absolute numbers of ILC3 and *Il22*$^{TdT+}$ ILC3 in small intestine lamina propria (F; n=3-5). Results are shown as the mean ± SEM (two-tailed Mann-Whitney test).

Figure S3

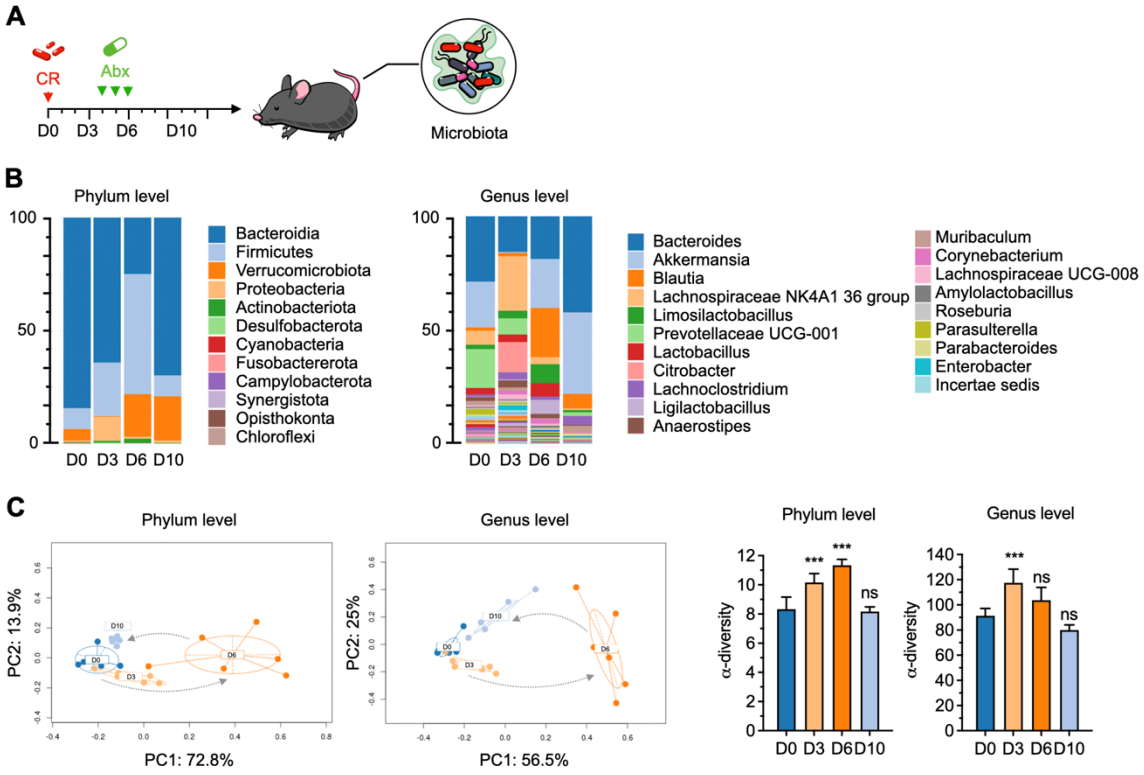

Fig. S3. Impact of CR infection and antibiotic treatment on intestinal microbiota
(**A**) C57BL/6 mice received ciprofloxacin (Abx; 100 mg/kg/day) by oral gavage and feces were collected before infection (day 0; D0) and at indicated time points after infection and antibiotic treatment. (**B**) Relative abundance of major bacterial phylum and genus in the fecal microbiota were quantified by 16S rRNA gene sequencing. (**C**) 16S rRNA operational taxonomic units (OTU) are clustered according to principal-coordinate (PC) analysis of untreated and treated mice. Percentage of variation, using Bray Curtis distance, are indicated on the *x* and *y* axes. The alpha diversity, shown as total observed OTU, in untreated and treated mice. Mean and standard error of mean (SEM) values indicated, and subgroups (n=6) are compared to control (D0, n=6) with nonparametric one-way ANOVA test followed by pairwise comparisons. Data are representative of one experiment. Results are shown as the mean ± SEM.**P<0.01; *** P<0.001.

Figure S4

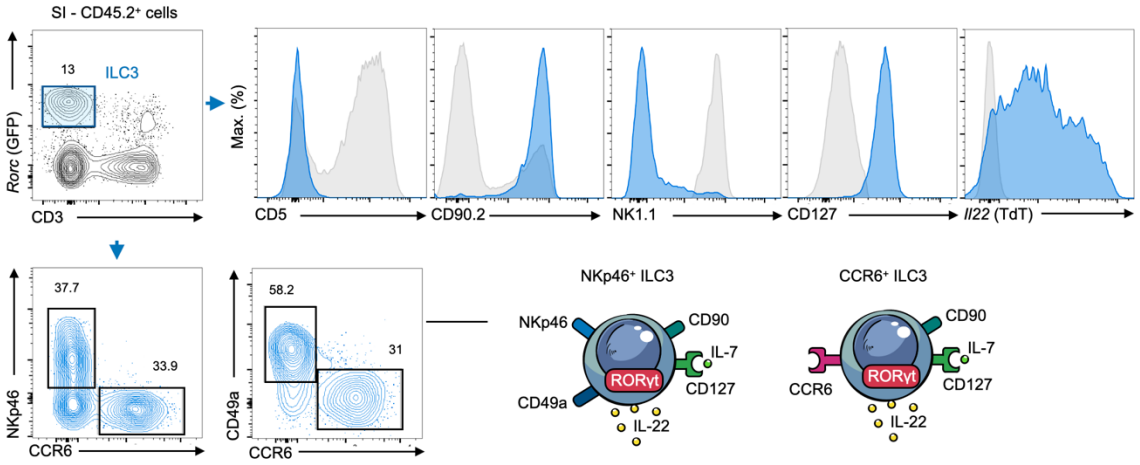

Fig. S4. Identification of small intestinal ILC3 by flow cytometry
Small intestine ILC3 were analyzed by flow cytometry and gated on CD45.2^{+}CD3^{-} *Rorc*$^{GFP+}$ cells. Representative flow cytometry plots of CCR6, CD127, CD49a, CD5, CD90.2, NK1.1, NKp46, and *Il22*^{TdT} expression in intestinal ILC3. A negative intestinal population (gray) is shown as a control for each marker: CD45.2^{+} CD3^{+} T cells for CD5; CD3^{-}CD5^{-}CD127^{-}NK1.1^{-}cells for CD90.2, CD127, and *Il22*^{TdT}; CD45.2^{+} CD3^{-} NKp46^{Hi} NK cells for NK1.1). All data are representative of three independent experiments with similar results.

Figure S5

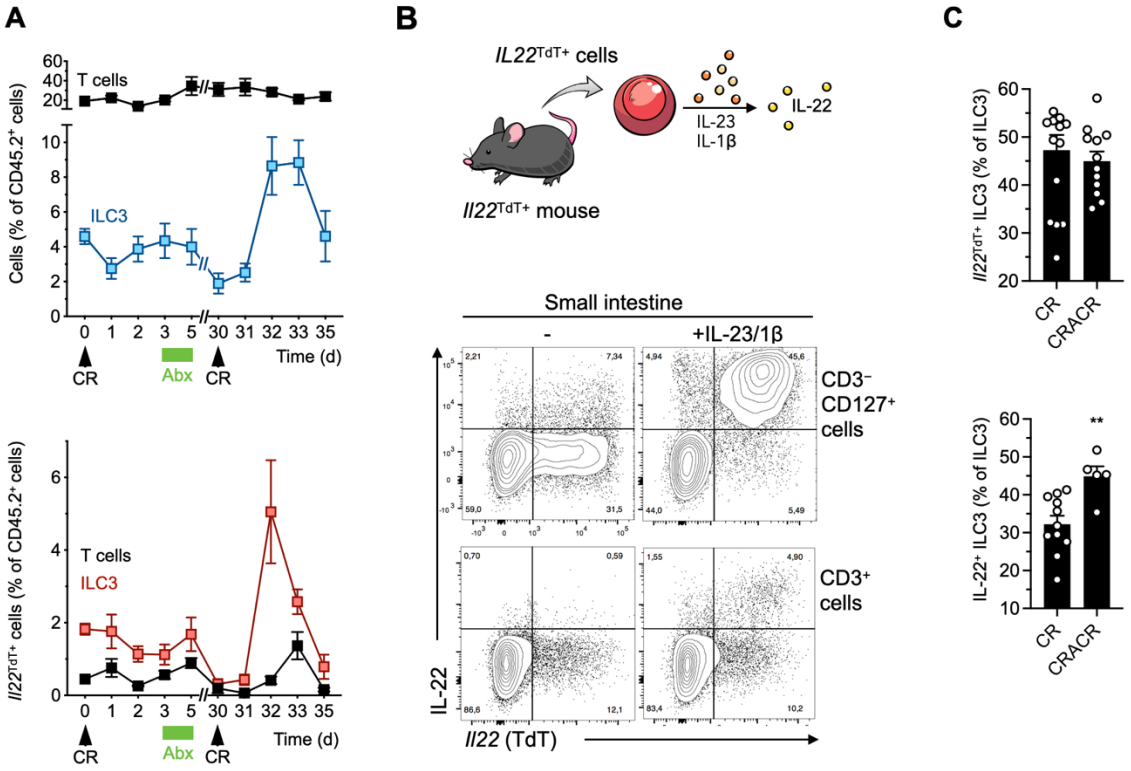

Fig. S5. Expression of *Il22*^{TdT} and IL-22 in intestinal ILC3 and T cells
(**A**) *Rorc*^{GFP}*Il22*^{TdT} reporter mice received ciprofloxacin (Abx; 100 mg/kg/day) after CR infection. One month later, the mice were reinfected with CR (CRACR). Frequency of total and *Il22*$^{TdT+}$ T cells and ILC3 were analyzed. Representative data of six independent analysis (n=4-12 for each time point). (**B**) Representative flow cytometry analysis of *Il22* (TdT) and IL-22 expression in CD3^{-} CD127^{+} cells and T cells (CD3^{+} cells) from *Il22*^{TdT} mice after ex vivo IL-23 and IL-1β stimulation. (**C**) Frequency of *Il22*$^{TdT+}$ (n=12-15) and IL-22^{+} ILC3 (n=5-11) in CR and CRACR mice. Data are representative of three independent experiments. Mean ± SEM (**P<0.01; two-tailed Mann-Whitney test).

Figure S6

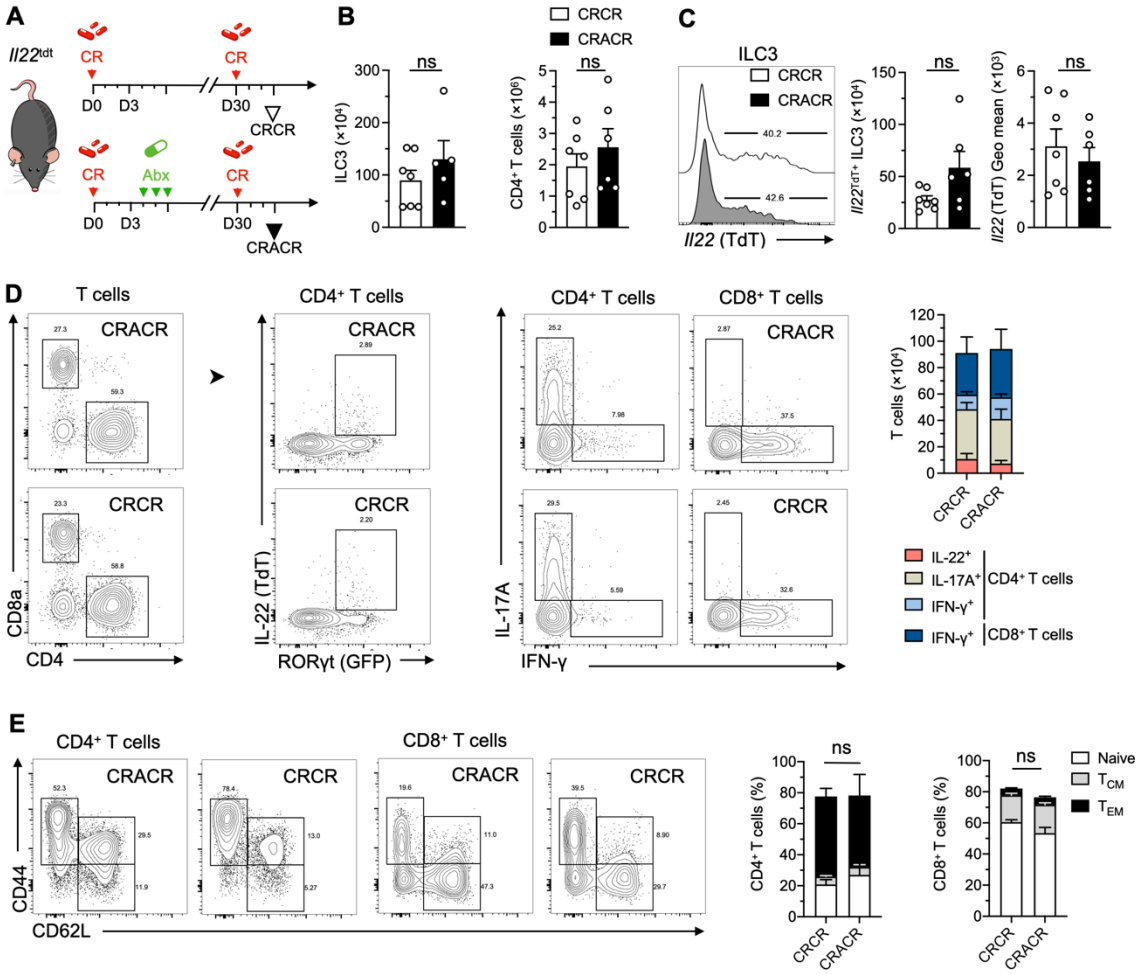

Fig. S6. ILC3 and T cell responses in CRCR and CRACR models

(**A** to **E**) *Il22*^{TdT} mice received water (CRCR) or ciprofloxacin (Abx; 100 mg/kg/day; CRACR) after CR infection. One month later, mice were reinfected with CR. (**B** to **E)** Absolute numbers of ILC3 and CD4$^+$ T cells (B; n=5-7), cytokine-producing ILC3 (numbers and frequencies; C; n=6-7), T cells (D; n=6-7), and tissue-resident T cell subsets (E; n=6-7) (T_{CM}, central memory CD44$^+$ CD62L$^+$ T cells; T_{EM}, effector memory CD44$^+$ CD62L$^-$ T cells; CD44$^-$ CD62L$^+$ naïve T cells) in small intestine lamina propria cells. Mean ± SEM (ns, not significant; two-tailed Mann-Whitney test).

Figure S7

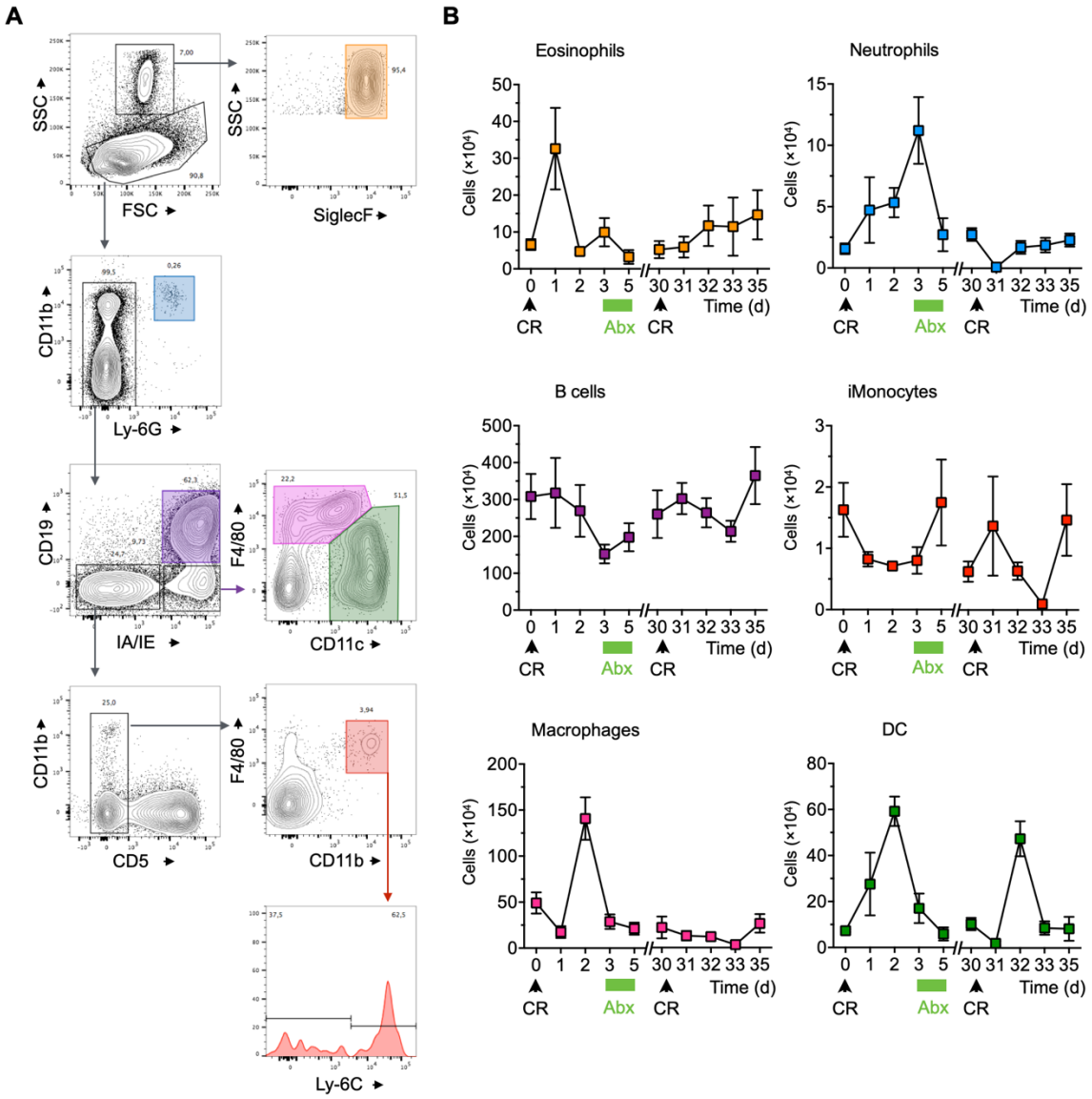

Fig. S7. Analysis of intestinal immune cells after bacterial infection
(**A**) Analysis of eosinophils ($SSC^{hi}CD45^{+}SiglecF^{+}$), neutrophils ($CD45^{+}CD11b^{+}Ly6G^{+}$), B cells ($CD45^{+}CD19^{+}MHCII^{+}$), macrophages ($CD45^{+}$ $CD19^{-}MHCII^{+}F4/80^{+}CD11c^{lo}$), dendritic cells (DC) ($CD45^{+}CD19^{-}MHCII^{+}F4/80^{lo}$ $CD11c^{hi}$), and monocytes ($CD45^{+}MHCII^{-}CD5^{-}CD11b^{+}F4/80^{+}Ly6C^{+/-}$). (**B**) Absolute numbers of immune cells in small intestine lamina propria (n=3 for each time point). Results are shown as means ± SEM.

Figure S8

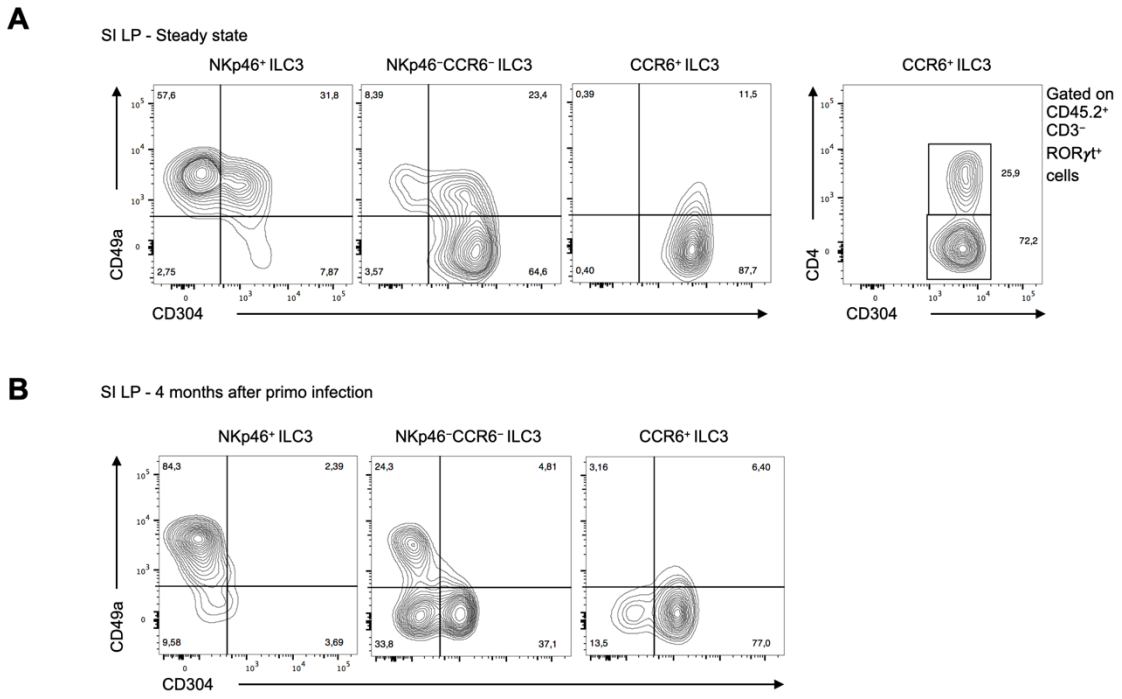

Fig. S8. **Expression of CD49a, CD304 and CD4 on cell surface of gut ILC3 subsets** (**A** and **B**) Expression of CD49a, CD304 (or Nrp1) and CD4 on ILC3 (CD45^{+} *Rorc*$^{GFP+}$ CD3^{-} cells) from small intestine *Rorc*^{GFP} *Il22*^{TdT} mice before *C. rodentium* infection (A) or 4 months after infection and 3 days after *C. rodentium* reinfection. Data are representative of three independent experiments.

Figure S9

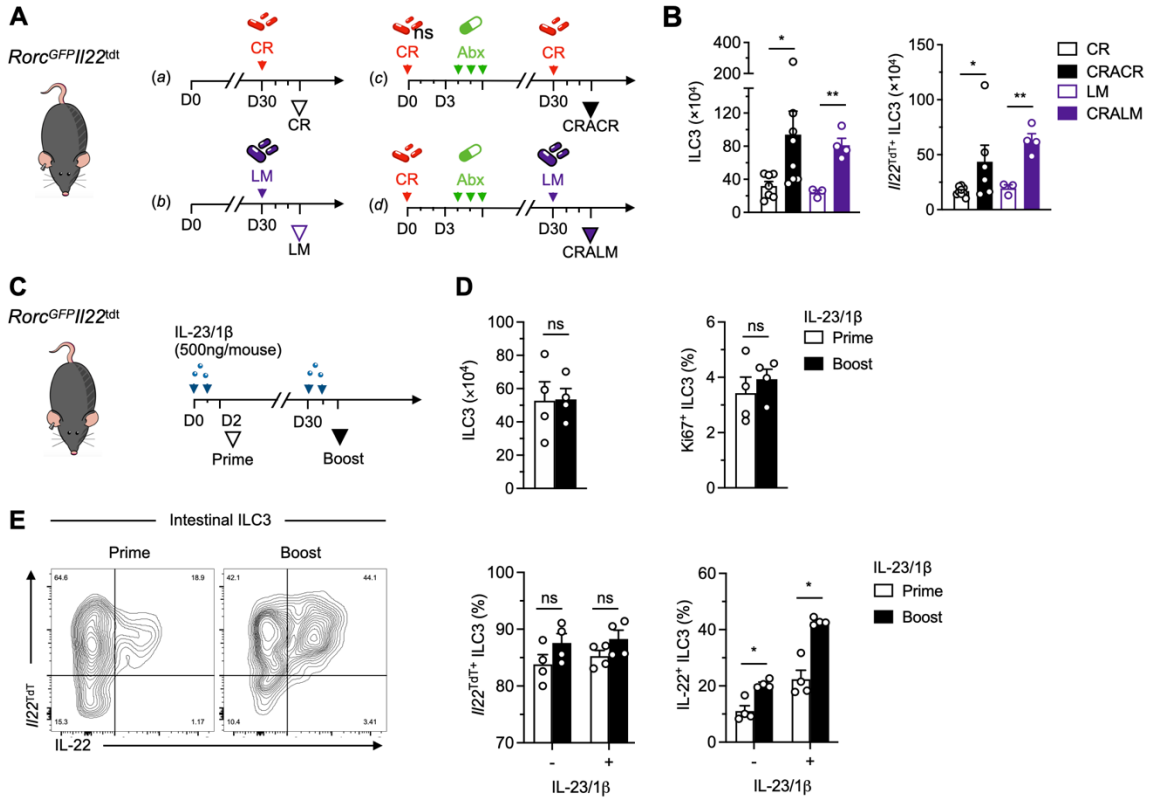

Fig. S9. ILC3 response to unrelated pathogen and cytokine challenge.
(**A**) *Rorc*^{GFP} *Il22*^{TdT} mice received ciprofloxacin (Abx; 100 mg/kg/day) after CR infection. One month later, the mice were reinfected with CR (CRACR) or *L. monocytogenes* (CRALM). Control groups were infected with CR *or L. monocytogenes* (LM) alone. (**B**) Intestinal ILC3 and *Il22*$^{TdT+}$ ILC3 were analyzed (n=3-8). (**C**) *Rorc*^{GFP} *Il22*^{TdT} mice received two i.p. injections of IL-23 and IL-1β. One month later, they received two i.p. injections of IL-23 and IL-1β. (**D** and **E**) Numbers of ILC3, percentages of Ki67^{+} and IL-22^{+} primed and boosted ILC3 were determined after 3 hours of restimulation with IL-23 and IL-1β (n=4). Data are representative of two independent experiments. Mean ± SEM (*P<0.05, ** P <0.01; two-tailed Mann-Whitney test).

Figure S10

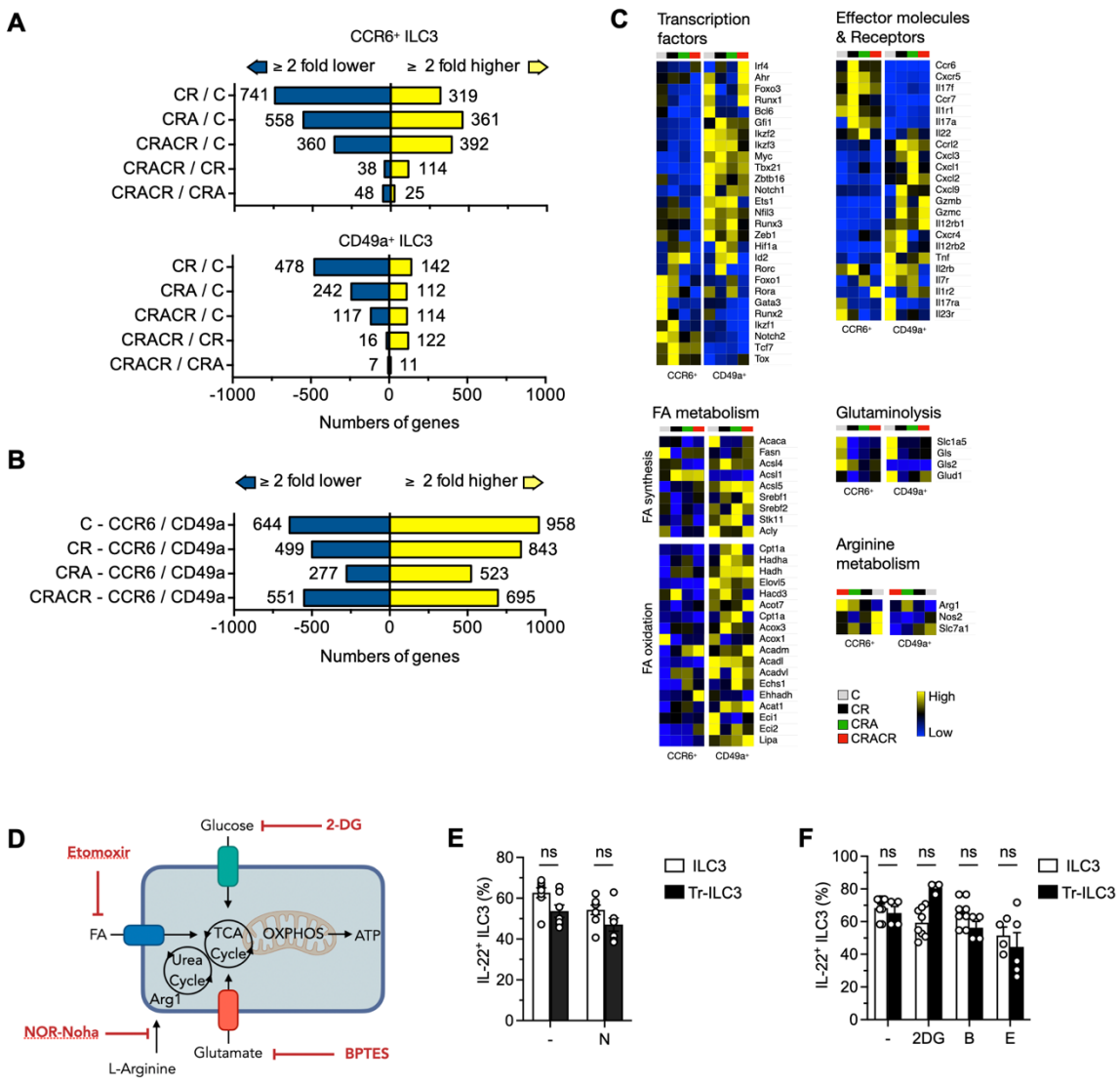

Fig. S10. RNA-seq analysis of ILC3 subsets

(**A** and **B**) Numbers of genes with a ≥ 2-fold decrease (blue) or increase (yellow) in expression between the indicated populations and conditions. (**C**) Heatmap showing differentially expressed genes in ILC3 subsets in the small intestine of C, CR, CRA and CRACR mice (n=3). (**D**) Schematic representation of metabolic pathways affected by inhibitors. (**E**) ILC3 and trained-ILC3 (Tr-ILC3), from C and CRACR mice respectively, were stimulated with IL-23 and IL-1β in the presence of the Arg1 inhibitor, Nor-NOHA (N). DMSO (-) was used as a control (n=7-8). (**F**) ILC3 and Tr-ILC3 (from C and CRACR mice) were cultured with 2-DG, B, E and N before stimulation with IL-23 and IL-1β and analysis of IL-22 protein expression (n=4-8). Mean ± SEM (E-F, two-tailed Mann-Whitney test).

References and Notes

1. L. V. Hooper, A. J. Macpherson, Immune adaptations that maintain homeostasis with the intestinal microbiota. *Nat. Rev. Immunol.* **10**, 159–169 (2010). doi:10.1038/nri2710 Medline

2. H. Spits, D. Artis, M. Colonna, A. Diefenbach, J. P. Di Santo, G. Eberl, S. Koyasu, R. M. Locksley, A. N. J. McKenzie, R. E. Mebius, F. Powrie, E. Vivier, Innate lymphoid cells—A proposal for uniform nomenclature. *Nat. Rev. Immunol.* **13**, 145–149 (2013). doi:10.1038/nri3365 Medline

3. G. F. Sonnenberg, D. Artis, Innate lymphoid cells in the initiation, regulation and resolution of inflammation. *Nat. Med.* **21**, 698–708 (2015). doi:10.1038/nm.3892 Medline

4. C. S. N. Klose, D. Artis, Innate lymphoid cells as regulators of immunity, inflammation and tissue homeostasis. *Nat. Immunol.* **17**, 765–774 (2016). doi:10.1038/ni.3489 Medline

5. M. L. Robinette, A. Fuchs, V. S. Cortez, J. S. Lee, Y. Wang, S. K. Durum, S. Gilfillan, M. Colonna, Immunological Genome Consortium, Transcriptional programs define molecular characteristics of innate lymphoid cell classes and subsets. *Nat. Immunol.* **16**, 306–317 (2015). doi:10.1038/ni.3094 Medline

6. N. Satoh-Takayama, C. A. J. Vosshenrich, S. Lesjean-Pottier, S. Sawa, M. Lochner, F. Rattis, J.-J. Mention, K. Thiam, N. Cerf-Bensussan, O. Mandelboim, G. Eberl, J. P. Di Santo, Microbial flora drives interleukin 22 production in intestinal NKp46^{+} cells that provide innate mucosal immune defense. *Immunity* **29**, 958–970 (2008). doi:10.1016/j.immuni.2008.11.001 Medline

7. G. F. Sonnenberg, L. A. Monticelli, M. M. Elloso, L. A. Fouser, D. Artis, CD4^{+} lymphoid tissue-inducer cells promote innate immunity in the gut. *Immunity* **34**, 122–134 (2011). doi:10.1016/j.immuni.2010.12.009 Medline

8. S. Buonocore, P. P. Ahern, H. H. Uhlig, I. I. Ivanov, D. R. Littman, K. J. Maloy, F. Powrie, Innate lymphoid cells drive interleukin-23-dependent innate intestinal pathology. *Nature* **464**, 1371–1375 (2010). doi:10.1038/nature08949 Medline

9. M. Cella, A. Fuchs, W. Vermi, F. Facchetti, K. Otero, J. K. M. Lennerz, J. M. Doherty, J. C. Mills, M. Colonna, A human natural killer cell subset provides an innate source of IL-22 for mucosal immunity. *Nature* **457**, 722–725 (2009). doi:10.1038/nature07537 Medline

10. H. Yoshida, K. Honda, R. Shinkura, S. Adachi, S. Nishikawa, K. Maki, K. Ikuta, S.-I. Nishikawa, IL-7 receptor α^{+} CD3^{-} cells in the embryonic intestine induces the organizing center of Peyer's patches. *Int. Immunol.* **11**, 643–655 (1999). doi:10.1093/intimm/11.5.643 Medline

11. R. E. Mebius, P. Rennert, I. L. Weissman, Developing lymph nodes collect CD4^{+}CD3^{-} LTβ^{+} cells that can differentiate to APC, NK cells, and follicular cells but not T or B cells. *Immunity* **7**, 493–504 (1997). doi:10.1016/S1074-7613(00)80371-4 Medline

12. S. Sawa, M. Lochner, N. Satoh-Takayama, S. Dulauroy, M. Bérard, M. Kleinschek, D. Cua, J. P. Di Santo, G. Eberl, RORγt^{+} innate lymphoid cells regulate intestinal homeostasis by integrating negative signals from the symbiotic microbiota. *Nat. Immunol.* **12**, 320–326 (2011). doi:10.1038/ni.2002 Medline

13. J. W. Collins, K. M. Keeney, V. F. Crepin, V. A. K. Rathinam, K. A. Fitzgerald, B. B. Finlay, G. Frankel, *Citrobacter rodentium*: Infection, inflammation and the microbiota. *Nat. Rev. Microbiol.* **12**, 612–623 (2014). doi:10.1038/nrmicro3315 Medline

14. R. Basu, D. B. O'Quinn, D. J. Silberger, T. R. Schoeb, L. Fouser, W. Ouyang, R. D. Hatton, C. T. Weaver, Th22 cells are an important source of IL-22 for host protection against enteropathogenic bacteria. *Immunity* **37**, 1061–1075 (2012). doi:10.1016/j.immuni.2012.08.024 Medline

15. C. Mullineaux-Sanders, J. W. Collins, D. Ruano-Gallego, M. Levy, M. Pevsner-Fischer, I. T. Glegola-Madejska, A. M. Sågfors, J. L. C. Wong, E. Elinav, V. F. Crepin, G. Frankel, *Citrobacter rodentium* relies on commensals for colonization of the colonic mucosa. *Cell Rep.* **21**, 3381–3389 (2017). doi:10.1016/j.celrep.2017.11.086 Medline

16. G. Eberl, S. Marmon, M. J. Sunshine, P. D. Rennert, Y. Choi, D. R. Littman, An essential function for the nuclear receptor RORγt in the generation of fetal lymphoid tissue inducer cells. *Nat. Immunol.* **5**, 64–73 (2004). doi:10.1038/ni1022 Medline

17. W. Shen, J. A. Hixon, M. H. McLean, W. Q. Li, S. K. Durum, IL-22-expressing murine lymphocytes display plasticity and pathogenicity in reporter mice. *Front. Immunol.* **6**, 662 (2016). Medline

18. K. Wolk, S. Kunz, E. Witte, M. Friedrich, K. Asadullah, R. Sabat, IL-22 increases the innate immunity of tissues. *Immunity* **21**, 241–254 (2004). doi:10.1016/j.immuni.2004.07.007 Medline

19. Y. Zheng, P. A. Valdez, D. M. Danilenko, Y. Hu, S. M. Sa, Q. Gong, A. R. Abbas, Z. Modrusan, N. Ghilardi, F. J. de Sauvage, W. Ouyang, Interleukin-22 mediates early host defense against attaching and effacing bacterial pathogens. *Nat. Med.* **14**, 282–289 (2008). doi:10.1038/nm1720 Medline

20. M. Cherrier, S. Sawa, G. Eberl, Notch, Id2, and RORγt sequentially orchestrate the fetal development of lymphoid tissue inducer cells. *J. Exp. Med.* **209**, 729–740 (2012). doi:10.1084/jem.20111594 Medline

21. W. Xu, D. E. Cherrier, S. Chea, C. Vosshenrich, N. Serafini, M. Petit, P. Liu, R. Golub, J. P. Di Santo, An $Id2^{RFP}$-reporter mouse redefines innate lymphoid cell precursor potentials. *Immunity* **50**, 1054–1068.e3 (2019). doi:10.1016/j.immuni.2019.02.022 Medline

22. E. L. Rawlins, C. P. Clark, Y. Xue, B. L. Hogan, The $Id2^{+}$ distal tip lung epithelium contains individual multipotent embryonic progenitor cells. *Development* **136**, 3741–3745 (2009). doi:10.1242/dev.037317 Medline

23. J. Ordovas-Montanes, S. Beyaz, S. Rakoff-Nahoum, A. K. Shalek, Distribution and storage of inflammatory memory in barrier tissues. *Nat. Rev. Immunol.* **20**, 308–320 (2020). doi:10.1038/s41577-019-0263-z Medline

24. S. Saeed, J. Quintin, H. H. D. Kerstens, N. A. Rao, A. Aghajanirefah, F. Matarese, S.-C. Cheng, J. Ratter, K. Berentsen, M. A. van der Ent, N. Sharifi, E. M. Janssen-Megens, M. Ter Huurne, A. Mandoli, T. van Schaik, A. Ng, F. Burden, K. Downes, M. Frontini, V. Kumar, E. J. Giamarellos-Bourboulis, W. H. Ouwehand, J. W. M. van der Meer, L. A. B. Joosten, C. Wijmenga, J. H. A. Martens, R. J. Xavier, C. Logie, M. G. Netea, H. G. Stunnenberg, Epigenetic programming of monocyte-to-macrophage differentiation and

trained innate immunity. *Science* **345**, 1251086 (2014). doi:10.1126/science.1251086 Medline

25. M. A. Cooper, J. M. Elliott, P. A. Keyel, L. Yang, J. A. Carrero, W. M. Yokoyama, Cytokine-induced memory-like natural killer cells. *Proc. Natl. Acad. Sci. U.S.A.* **106**, 1915–1919 (2009). doi:10.1073/pnas.0813192106 Medline

26. J. C. Sun, J. N. Beilke, L. L. Lanier, Adaptive immune features of natural killer cells. *Nature* **457**, 557–561 (2009). doi:10.1038/nature07665 Medline

27. I. Martinez-Gonzalez, L. Mathä, C. A. Steer, M. Ghaedi, G. F. T. Poon, F. Takei, Allergen-experienced group 2 Innate lymphoid cells acquire memory-like properties and enhance allergic lung inflammation. *Immunity* **45**, 198–208 (2016). doi:10.1016/j.immuni.2016.06.017 Medline

28. O. Disson, C. Blériot, J.-M. Jacob, N. Serafini, S. Dulauroy, G. Jouvion, C. Fevre, G. Gessain, P. Thouvenot, G. Eberl, J. P. Di Santo, L. Peduto, M. Lecuit, Peyer's patch myeloid cells infection by *Listeria* signals through gp38^{+} stromal cells and locks intestinal villus invasion. *J. Exp. Med.* **215**, 2936–2954 (2018). doi:10.1084/jem.20181210 Medline

29. R. J. W. Arts, L. A. B. Joosten, M. G. Netea, Immunometabolic circuits in trained immunity. *Semin. Immunol.* **28**, 425–430 (2016). doi:10.1016/j.smim.2016.09.002 Medline

30. G. R. Bantug, L. Galluzzi, G. Kroemer, C. Hess, The spectrum of T cell metabolism in health and disease. *Nat. Rev. Immunol.* **18**, 19–34 (2018). doi:10.1038/nri.2017.99 Medline

31.J. Muri, M. Kopf, Redox regulation of immunometabolism. *Nat. Rev. Immunol.* **21**, 363–381 (2021). doi:10.1038/s41577-020-00478-8 Medline

32. R. Geiger, J. C. Rieckmann, T. Wolf, C. Basso, Y. Feng, T. Fuhrer, M. Kogadeeva, P. Picotti, F. Meissner, M. Mann, N. Zamboni, F. Sallusto, A. Lanzavecchia, L-Arginine modulates T cell metabolism and enhances survival and anti-tumor activity. *Cell* **167**, 829–842.e13 (2016). doi:10.1016/j.cell.2016.09.031 Medline

33. L. A. Monticelli, M. D. Buck, A.-L. Flamar, S. A. Saenz, E. D. Tait Wojno, N. A. Yudanin, L. C. Osborne, M. R. Hepworth, S. V. Tran, H.-R. Rodewald, H. Shah, J. R. Cross, J. M. Diamond, E. Cantu, J. D. Christie, E. L. Pearce, D. Artis, Arginase 1 is an innate lymphoid-cell-intrinsic metabolic checkpoint controlling type 2 inflammation. *Nat. Immunol.* **17**, 656–665 (2016). doi:10.1038/ni.3421 Medline

34. G. Caputa, A. Castoldi, E. J. Pearce, Metabolic adaptations of tissue-resident immune cells. *Nat. Immunol.* **20**, 793–801 (2019). doi:10.1038/s41590-019-0407-0 Medline

35. M. D. Buck, D. O'Sullivan, E. L. Pearce, T cell metabolism drives immunity. *J. Exp. Med.* **212**, 1345–1360 (2015). doi:10.1084/jem.20151159 Medline

36. L. Dumoutier, M. de Heusch, C. Orabona, N. Satoh-Takayama, G. Eberl, J.-C. Sirard, J. P. Di Santo, J.-C. Renauld, IL-22 is produced by γC-independent CD25^{+} CCR6^{+} innate murine spleen cells upon inflammatory stimuli and contributes to LPS-induced lethality. *Eur. J. Immunol.* **41**, 1075–1085 (2011). doi:10.1002/eji.201040878 Medline

37. S. Wiles, K. M. Pickard, K. Peng, T. T. MacDonald, G. Frankel, In vivo bioluminescence imaging of the murine pathogen *Citrobacter rodentium*. *Infect. Immun.* **74**, 5391–5396 (2006). doi:10.1128/IAI.00848-06 Medline

38. N. Satoh-Takayama, N. Serafini, T. Verrier, A. Rekiki, J.-C. Renauld, G. Frankel, J. P. Di Santo, The chemokine receptor CXCR6 controls the functional topography of interleukin-22 producing intestinal innate lymphoid cells. *Immunity* **41**, 776–788 (2014). doi:10.1016/j.immuni.2014.10.007 Medline

39. P. Gonçalves, S. El Daker, F. Vasseur, N. Serafini, A. Lim, O. Azogui, H. Decaluwe, D. Guy-Grand, A. A. Freitas, J. P. Di Santo, B. Rocha, Microbiota stimulation generates LCMV-specific memory $CD8^+$ T cells in SPF mice and determines their TCR repertoire during LCMV infection. *Mol. Immunol.* **124**, 125–141 (2020). doi:10.1016/j.molimm.2020.05.012 Medline

40. J. J. Quereda, O. Dussurget, M.-A. Nahori, A. Ghozlane, S. Volant, M.-A. Dillies, B. Regnault, S. Kennedy, S. Mondot, B. Villoing, P. Cossart, J. Pizarro-Cerda, Bacteriocin from epidemic *Listeria* strains alters the host intestinal microbiota to favor infection. *Proc. Natl. Acad. Sci. U.S.A.* **113**, 5706–5711 (2016). doi:10.1073/pnas.1523899113 Medline

41. L. Surace, J.-M. Doisne, P. Escoll, S. Marie, V. Dardalhon, C. Croft, A. Thaller, D. Topazio, A. Sparaneo, A. Cama, O. Musumeci, A. d'Ecclesia, C. Buchrieser, N. Taylor, J. P. Di Santo, Polarized mitochondria as guardians of NK cell fitness. *Blood Adv.* **5**, 26–38 (2021). doi:10.1182/bloodadvances.2020003458 Medline